

pubs.acs.org/Macromolecules Article

Simple Approach to Synthesize Carbohydrate-based Janus-Type Bottlebrush Copolymers and Their Self-Assemblies in Sub-5 nm Features in Thin Films

Muhammad Mumtaz,* Daniel Hermida Merino, Eduardo Solano, Wen-Chang Chen, and Redouane Borsali*



Cite This: Macromolecules 2024, 57, 9595-9605



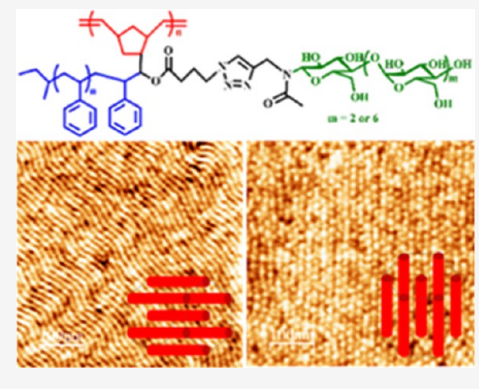
ACCESS

III Metrics & More

Article Recommendations

Supporting Information

ABSTRACT: We demonstrate an original and simple route to synthesize oligosaccharides-based Janus-type bottlebrush block copolymers (BBCPs) with the combination of anionic polymerization, ring-opening metathesis polymerization, and click chemistry techniques following grafting-through and grafting-to approach. These Janus-type BBCPs having different molecular weights of side chains and backbone lengths undergo phase-segregation under conventional solvent vapor annealing (SVA) for 14–60 h or high temperature solvent vapor annealing (HTSVA) using μ -wave energy for 1 min, into long-range order sub-5 nm (half-pitch) periodic nanodomains in their thin films. This simple strategy could be used for large-scale production of Janus-type BBCPs, and side chains on either side of BBCPs could be replaced by a variety of other polymer systems. By replacing the oligosaccharides branches by other polymer systems like polylactide, polycaprolactone, or poly(ethylene oxide), we could further simplify this approach and reduce



the number of steps (2 or 3) to reach the final product, i.e., from synthesis of macromonomer to final Janus-type BBCPs. It is noteworthy that it is the first report on achieving sub-5 nm nanofeatures in thin films using Janus-type BBCPs.

INTRODUCTION

Block copolymer (BCP) materials have attracted a lot of research interest, thanks to their ability to self-assemble into many useful periodic nanofeatures such as hexagonal cylinders, cubic spheres, alternating lamellae, and bicontinuous gyroids, ^{1,2} These nanostructures have shown a wide range of applications in nanolithography, ^{3,4} electronic and energy devices, ^{5–9} and nanoscale templating and patterning, ^{10,11} leading to important developments in the semiconductor and many other industries.

While strategies for obtaining long-range lateral ordering of microdomains with dimensions between 10 and 100 nm have been well studied, achieving well-ordered microdomains in the sub-10 nm regime remains challenging. The interest in nanofabrication via BCP self-assembly has motivated studies of diverse block architectures, such as multiblocks and bottlebrushes, to overcome the limitations of diblock copolymers and extend the available microdomain geometries. Conventional "A-block-B" diblock bottlebrush copolymers (BBCPs) consist of a backbone with side chains of each block occupying different regions of the backbone and exhibit large molecular size, densely grafted side chains and a wormlike conformation. These conventional diblock BBCPs with high molecular weight have tendency to undergo rapid microphase separation due to the lack of entanglement and thus reduced kinetic barrier for self-assembly. However,

the self-assembled microdomain sizes achievable via BBCPs are much larger than that obtained from their linear analogs, making them attractive candidates for applications such as photonic crystals. ^{17,18}

In BCPs with moderate intersegment repulsion, typically reflected by a relatively low value of the Flory–Huggins interaction parameter (χ), a high N (degree of polymerization) value that is required to ensure a sufficiently large thermodynamic driving force for the formation of well-ordered nanostructures inevitably results in a large nanodomain size. A prevailing approach to scaling down nanodomains is based on the design of high- χ BCPs^{19–26} that allow for the creation of ordered nanostructures with significantly reduced N. The introduction of high- χ segments in low-N BCPs to compensate for the loss in the driving force for self-assembly may interfere with other properties, such as thermomechanical behaviors and processability, that are essential for a chosen application.

Received: February 16, 2024
Revised: September 12, 2024
Accepted: September 30, 2024
Published: October 5, 2024





Scheme 1. Synthesis of Janus-Type Bottle-Brush Block Copolymers

In order to reduce the domain spacing in high- χ copolymers without sacrificing their thermomechanical properties and processability, which are key for their large-scale industrial applications, a new class of copolymers named Janus-type BBCPs have been developed. Janus-type BBCPs are a class of special molecular brushes, which have two immiscible side chains also called "A-branch-B" on the repeating unit of the backbone. In contrast to the conventional linear BCPs and BBCPs, the microdomain period of Janus-type "A-branch-B" BBCPs scales with the length of the side chains instead of the overall backbone length. Therefore, ultrasmall period patterns with diverse morphologies can be realized from high-MW Janus-type BBCPs by tuning the side chain length.

However, the synthesis of these Janus-type BBCPs requires multistep reactions and complex purifications steps, therefore restricting their large-scale production for desired applications. Hence, new strategies are needed to simplify their synthesis.

Ross and co-workers³¹ have reported the self-assemblies of Janus-type "PS-branch-PDMS" BBCP using a topographical templating technique that exhibited 22 nm periodic cylindrical microdomains with long-range order under solvent vapor annealing (SVA). Interestingly, Guo et al.²⁷ have described the synthesis and self-assemblies of PDMS-branch-PLA BBCP into ultrasmall nanodomains (2.8 nm half-pitch) in bulk. To the best of our knowledge, the self-assemblies of Janus-type BBCP into sub-5 nm nanofeatures (half-pitch) in their thin films have never been reported in the literature.

Herein, we report a straightforward strategy to synthesize well-defined oligosaccharide-based Janus-type BBCPs by the combination of grafting-through and grafting-to approach, in three main steps using anionic polymerization, ring-opening metathesis polymerization (ROMP), and click chemistry. These Janus-type BBCP self-assemble in their thin films on a naked silicon substrate into nanodomains as small as sub-5 nm. The effects of the molecular weights of the PS side chain and oligosaccharide chain lengths as well as the Janus BBCPs backbone length on the size, morphology, and orientation of nanofeatures have been studied. Thin films were annealed using conventional SVA at room temperature for 14-60 h and high temperature solvent vapor annealing (HTSVA)³² for 1 min using microwave energy. The effect of solvent composition, duration, and solvent annealing technique on the thin films' self-segregation behavior has been described in

detail. The morphological behavior of Janus BBCPs in their thin films was studied by taking their atomic force microscopy (AFM) images and grazing incidence small-angle X-ray scattering (GISAXS) measurements.

RESULTS AND DISCUSSION

Synthesis of Janus Copolymers. The oligosaccharide-based Janus-type BBCPs were prepared by the combination of anionic, ROMP, and click chemistry, as illustrated in Scheme 1.

In order to realize the synthesis of Janus-type block copolymers with immiscible side chains, several samples of ω -(1-bicyclo [2.2.1]hept-5ene-2yl)-1-methanol)-functionalized polystyrene (PSNb–OH) with different molecules were prepared by anionic polymerization of styrene in toluene accompanied by the addition of bicyclo[2.2.1]hept-5-ene-2-carboxaldehyde to terminate the reaction. The characteristics of PSNb–OH samples are summarized in Table S1. As confirmed from their size exclusion chromatography (SEC) characterization (Figure S1), well-defined PSNb–OH polymer samples with controlled molar mass and narrow dispersity were obtained during this process.

The 1 H NMR spectra of the PSNb–OH samples are shown in Figure S2. The molar mass of the PSNb–OH could also be determined by the relative integration of the peaks present at 0.59–0.76 ppm due to two methyl groups from initiator to the peaks arising at 6.34–7.50 ppm due to the styrene ring in the 1 H NMR spectra of PSNb–OH samples and is in close agreement with molecular weight determined by SEC in DMF using a polystyrene standard. The presence of peaks at 5.48–6.24 ppm due to the (-CH=CH-) moiety of the norbornene ring confirms the end group functionalization.

The PSNb-OH samples were then treated with 4-bromobutyryl chloride in CH_2Cl_2 in the presence of Pyridine to obtain ω -(1-bicyclo[2.2.1]hept-5ene-2yl)-1-methyl-4-bromobutanoate) polystyrene (PSNb-BuBr). The ¹H NMR spectrum of a PSNb-BuBr sample is shown in Figure S3. The appearance of a peak at 3.43 ppm, characteristic of the ($-CH_2Br$) group, confirms the end group modification.

These PSNb-BuBr macromonomer samples were then subjected to ROMP with the desired degree of polymerization. The disappearance of the peaks at 5.48-6.24 ppm due to the (-CH=CH-) moiety of the norbornene ring accompanied by the appearance of a new broad peak at 5.0 ppm due to the

(-CH=CH-) moiety of the polynorbornene backbone in the ^IH NMR spectrum (Figure S4) of PPSNb-BuBr and a clear shift in the position of SEC curve to higher molecular weight (Figure S5) confirm the ring opening polymerization of the PSNb-BuBr macro-monomer. The characteristics of the PPSNb-BuBr samples prepared in this study are summarized in Table S2. As is evident from their SEC traces (Figure S6), well-defined PPSNb-BuBr samples with narrow size distribution were obtained during ring opening polymerization.

These PPSNb-BuBr samples were then treated with excess of NaN $_3$ in DMF to 60 °C overnight in order to introduce azido functionality. The complete displacement of the peak present at 3.35 ppm due to the $-\mathrm{CH}_2\mathrm{Br}$ group to 3.19 ppm in the $^1\mathrm{H}$ NMR (Figure S7) and appearance of a new peak at 2100 cm $^{-1}$ in the FTIR spectrum of PPSNb-BuN $_3$ revealed the full azido functionalization.

Finally, Janus-type bottlebrush copolymers were prepared using the grafting-to approach by click reaction of azido end-functionalized PPSNb-BuN $_3$ with acetylene end-functionalized oligosaccharides (MT-C \equiv CH, and MH-C \equiv CH) in DMF in the presence of copper nanopowder as a catalyst. The complete disappearance of the absorption band at \sim 2100 cm $^{-1}$ in the FTIR spectrum due to the azido group confirmed the quantitative conversion (Figure S8).

The block copolymers were further characterized by ¹H NMR spectroscopy and SEC. The ¹H NMR spectrum of Janus-02 is shown in Figure 1. The appearance of signals

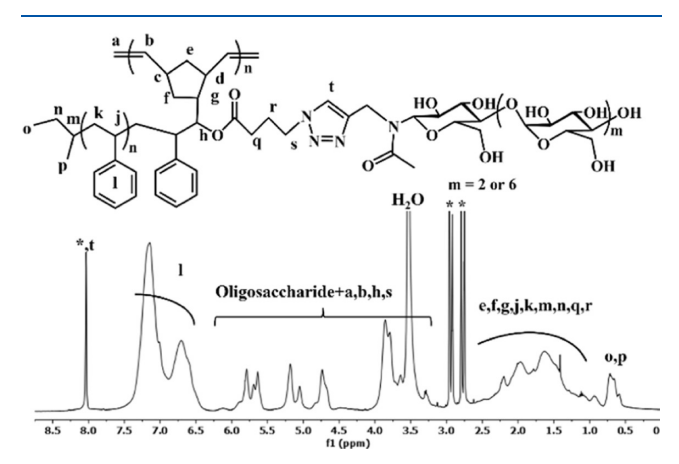


Figure 1. ¹H NMR spectrum of PPSNb-BuMH-02 (Janus-02, Table 1) in DMF- d_7 (400 MHz) at 25 °C.

positioned at 6.35–7.50 and 6.2–3.80 ppm due to styrene of the polystyrene backbone and oligosaccharides, respectively, confirmed the formation of Janus-type copolymers. The composition of copolymers could be determined by relative integration of the signals located at 6.35–7.50 ppm due to the styrene ring of the polystyrene backbone and at 5.18 ppm due to C1 protons of the oligosaccharide units.

The SEC analysis revealed the clear shift of the elution peak toward the higher molecular weight region upon the click reaction, which is clear evidence of the successful click reaction to form the desired copolymers (Figure S9). As is apparent from the SEC traces (Figures 2 and S10), well-defined Janus copolymers with narrow size distribution were prepared. The SEC curves follow their increasing molecular weight trends except Janus-03 and Janus-12 and are probably attributed to their difference in PS block molecular weight. When SEC

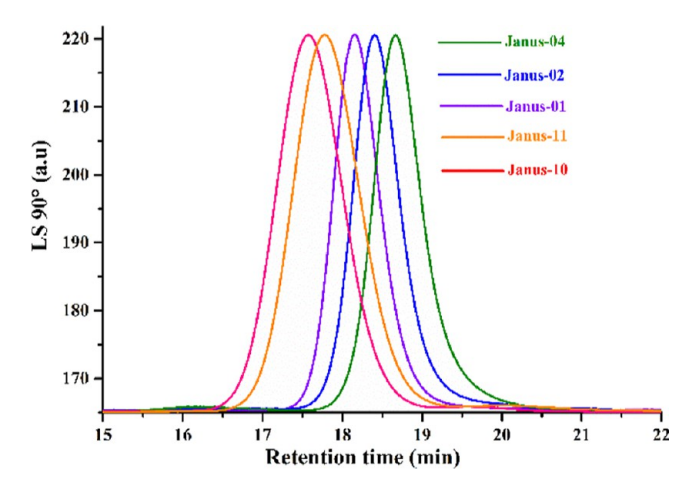


Figure 2. SEC traces of Janus-type BBCPs (Table 1) using DMF as an eluent at 40 $^{\circ}$ C.

traces of these samples were drawn separately, they follow their increasing molecular weight trend (Figure S10).

The characteristics of the different Janus copolymer samples are summarized in Table 1. As is evident from Table 1, the experimentally calculated molecular weight is in close agreement with theoretical molecular weights. Moreover, the overall experimentally obtained composition is very close to the expected values. A small difference from the expected values could be the result of micellization of the copolymers in solution during the NMR measurement, in which a small portion of the oligosaccharide is not accessible. Otherwise, their FTIR spectra showed full conversion of azido functions Figure S11.

Self-Assemblies of Janus Copolymers in Thin Films.

In order to investigate the self-assembly behavior of Janus-type bottle-brush copolymers (BBCPs) with different molecular weights and compositions, their thin films were prepared on freshly treated silicon wafers by the spin coating process. Plasma-treated silicon wafers facilitated the formation of uniform BBCP films due to the favorable interaction between the carbohydrate segments and the wafer's hydrophilic surface when the BBCPs, dissolved in DMF (a polar organic solvent), were subjected to the spin-coating process. In contrast, dewetting occurred when pristine silicon wafers were used. Film thickness, measured by reflectometry using a F-20 instrument from FILMETRICS, was found to be between 35 and 40 nm. These thin films were then subjected to conventional SVA and high temperature solvent annealing (HTSVA) using microwave energy. The self-assembly of Janus BBCP thin films was promoted by exposing the samples for 14-60 h to a THF/H₂O (1:1 or 3:1, w/w) saturated atmosphere for conventional solvent annealing at room temperature. On the other hand, BBCP thin films were annealed for only 1 min at 160 °C using μ-wave energy (HTSVA). THF/H₂O mixtures have been chosen as the solvent system since THF is a good solvent for PS and H2O is a good solvent for oligosaccharides. Therefore, the vapor produced from the THF/H₂O mixtures imparts mobility to both blocks of the BBCPs through the sample swelling, which is necessary to enable rearrangement and enhanced ordering of the self-assembled BBCPs thin films.

The 2D-GISAXS patterns of the thin films of Janus 1 (DP = 25, $M_{\rm n}^{\rm PS}$ = 2 kDa) prepared at different annealing times and solvent composition along with their corresponding AFM

Table 1. Characteristics of Janus-Type Copolymer Samples

sample	MM/I feed ratio	$M_{\rm n}$ of MM (1 H NMR) (2 mol)	Conv.a	sugar type MH/MT	$M_{\rm n}^{\rm totalb}$ of Janus-type BBCPs (theo.) kg/mol	$M_{ m n}^{ m total}$ of Janus-type BBCPs (SEC) kg/mol	Ð	$f_{ m mol}^{ m PS}$ d	$f_{ m V}^{ m PS}$ e	morphology ^f	domain spacing (nm)
Janus-01	25/1	2200	99	MH	86.4	102.0	1.04	0.50	0.67	CYL	13.6
Janus-02	25/1	1750	88	MH	64.02	69.20	1.13	0.55	0.65	CYL	12.7
Janus-03	25/1	5800	92	MH	133.40	106.25	1.02	0.60	0.90	CYL	14.6
Janus-04	25/1	1750	88	MT	49.7	72.4	1.04	0.57	0.85	CYL	8.3
Janus-10	100/1	1750	93	MH	270.63	221.16	1.07	0.50	0.61	CYL	13.0
Janus-11	100/1	1750	93	MT	210.18	151.6	1.02	050	0.81	CYL	9.4
Janus-12	25/1	3330	92	MH	104.90	94.3	1.04	0.50	0.77	CYL	15.0

"Obtained by the relative integration of monomer and polymer peaks in SEC traces using UV detector at 280 nm. "Theoretical molecular weight was determined by initial macromonomer (MM) to initiator (I) ratio and their conversion. "The molar mass of Janus BBCP was determined by SEC using light scattering putting dn/dc values for copolymers as 0.126 mL/g. "The molar composition of the Janus BBCP copolymer was determined by the relative integration of the signals located at 5.16 ppm due to C1 protons of oligosaccharides and 6.30–7.35 ppm phenyl ring of polystyrene. "The volume fraction of BBCP was determined using polymer densities values of 1.05, 1.36, and 1.80 for PS, MH, and MT, respectively. "Estimated from their respective 2D-GISAXS patterns of their thin films annealed in the 1:1 THF/H₂O SVA system for 24 h. [MM = macromonomer (PSNb-BuBr), Conv. = conversion, MH = maltoheptaose, MT = maltotriose, Theo. = theoretical, f_{mol} = molar fraction, f_v = volume fraction, CYL = cylinders].

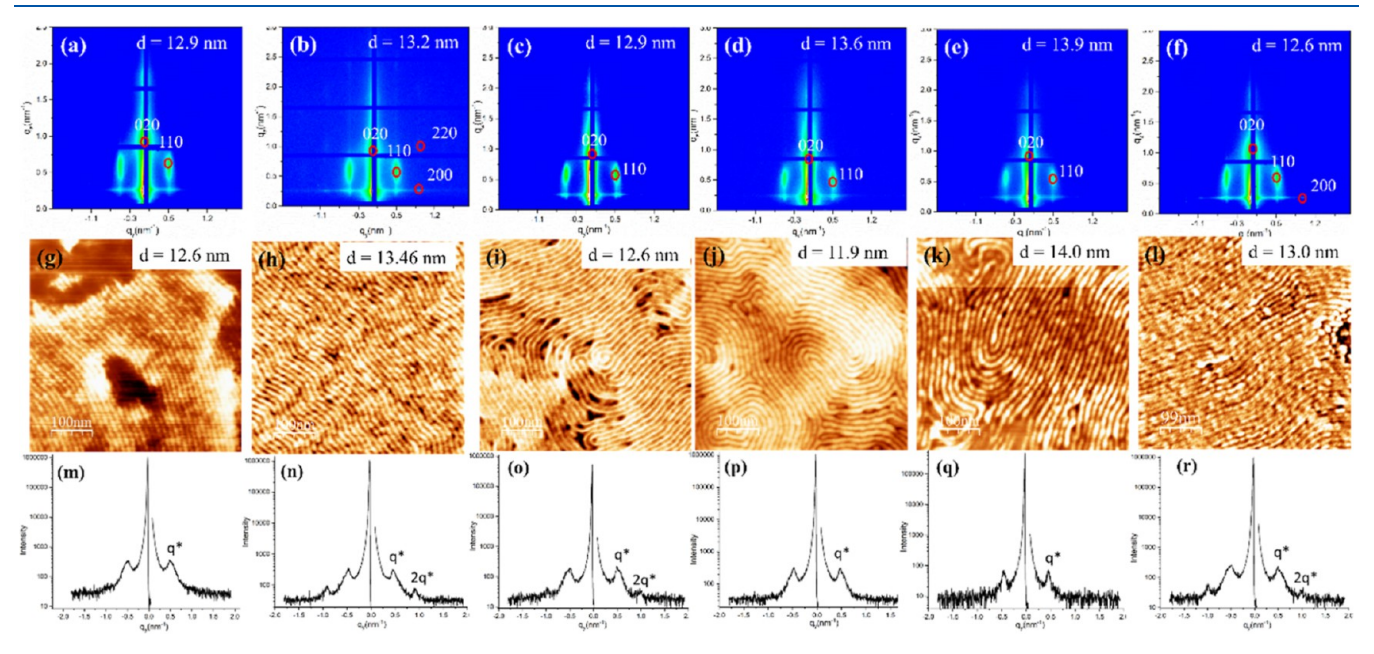


Figure 3. 2D-GISAXS of the PPSNb-BuMH-01 (Janus-01, Table 1) thin films annealed in different solvent vapor compositions and times: (a) THF/H₂O, 1:1, 14 h, (b) THF/H₂O, 1:1, 24 h, (c) THF/H₂O, 1:1, 60 h, (d) THF/H₂O, 3:1, 14 h, (e) THF/H₂O, 3:1, 24 h, and (f) THF/H₂O, 3:1, 60 h. (g–l) Their corresponding AFM images and (m–r) their respective GISAXS intensity cuts along the horizontal q_y direction taken around the Yoneda band d = domain spacing.

images are shown in Figure 3. As is apparent from Figure 3, well-defined nanofeatures are obtained in each case independent of the annealing conditions. The 2D-GISXAS scattering pattern of these samples reveals the presence of in-plane hexagonally packed carbohydrate cylinders (carbohydrate cylinders embedded in PS matrix), which is also supported by their corresponding AFM images, which show the presence of phase-separated fingerprint structures.

The domain spacing of these HEX cylinders was determined by their primary scattering peaks (q_y^*) using the relation $d = 2\pi/q^*$ and was shown in their corresponding images and is in close agreement with size measured by AFM.

The overall ordering in the thin films improves as the annealing times increases from 14 to 60 h in each case, as indicated in their AFM images. The presence of higher order scattering in 2D-GISAXS of the samples annealed in the presence of a solvent mixture with higher THF content shows

the presence of longer order and improved self-assembly in these conditions. The higher order obtained in this solvent mixture with a higher amount of PS as compared to oligosaccharides and THF is a good solvent for PS, which improves the chain mobility during self-segregation, resulting in an improvement in the order.

In order to study the effect of volume fraction of polystyrene on the self-assembly behavior of the Janus BBCPs in their thin films, another example with lower PS molecular weight $(M_n^{PS} = 1.6 \text{ kDa}, \text{lowest}$ in this study) was prepared (Janus-02, Table 1). The thin films of Janus-02 were annealed in identical conditions as described above. The resulting 2D-GISAXS patterns and their corresponding AFM images are shown in Figure 4.

Similar to this, 2D-GISAXS scattering patterns and AFM images of the thin films corroborated the self-segregation to HEX cylindrical morphologies. It is pertinent to mention here

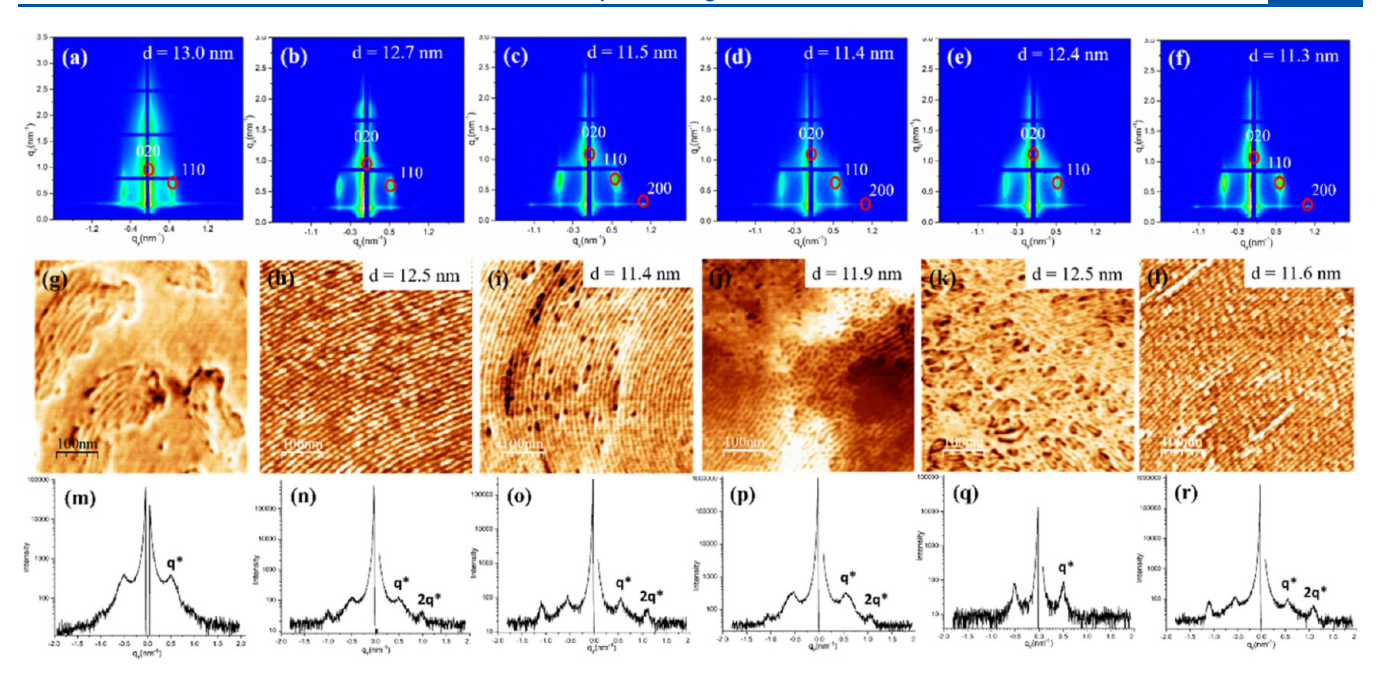


Figure 4. 2D-GISAXS of the PPSNb-BuMH-02 (Janus-02, Table 1) thin films annealed in different solvent vapor compositions and times: (a) THF/H₂O, 1:1, 14 h, (b) THF/H₂O, 1:1, 24 h, (c) THF/H₂O, 1:1, 60 h, (d) THF/H₂O, 3:1, 14 h, (e) THF/H₂O, 3:1, 24 h, and (f) THF/H₂O, 3:1, 60 h. (g–l) Their corresponding AFM images and (m–r) their respective GISAXS intensity cuts along the horizontal q_y direction taken around the Yoneda band.

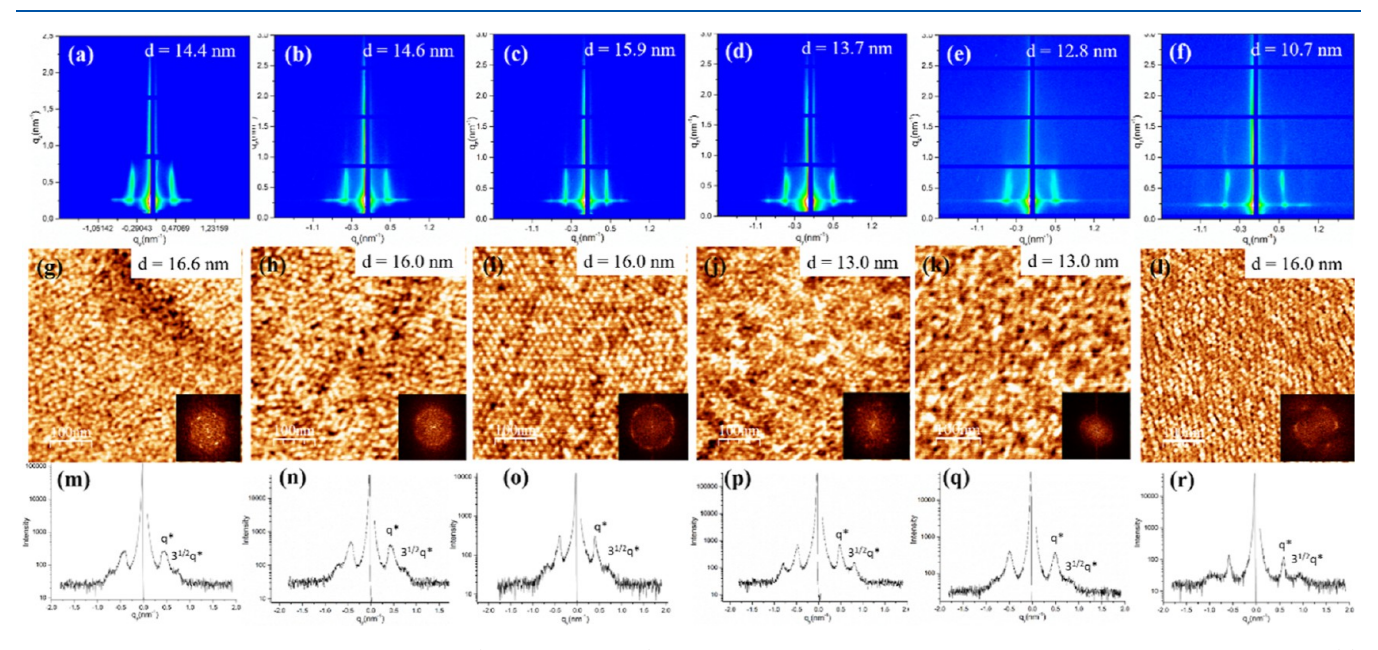


Figure 5. 2D-GISAXS of the PPSNb-BuMH-03 (Janus-03, Table 1) thin films annealed in different solvent vapor compositions and times: (a) THF/H₂O, 1:1, 14 h, (b) THF/H₂O, 1:1, 24 h, (c) THF/H₂O, 1:1, 60 h, (d) THF/H₂O, 3:1, 14 h, (e) THF/H₂O, 3:1, 24 h, and (f) THF/H₂O, 3:1, 60 h. (g–l) Their corresponding AFM images and (m–r) their respective GISAXS intensity cuts along the horizontal q_y direction taken around the Yoneda band.

that molar mass of PS branch (1.6 kDa) is very close to the MH branch (1.2 kDa) and one can expect the formation of lamellar morphology, but cylindrical morphologies were observed independent of the above-mentioned solvent annealing conditions. This could be the result of higher THF vapor pressure in the mixture due to its higher volatility caused by its lower boiling point as compared to $\rm H_2O$. As a result, PS swelled more as compared to oligosaccharides, resulting in the increase in the volume fraction of PS, leading to cylindrical morphologies in this case. The domain size calculated using

the primary scattering peak of each sample is close agreement with AFM.

As it is evident from AFM images in Figure 4, the improvement in the long-range order is observed with increasing solvent annealing time, which is further supported by the presence of higher order peaks in their corresponding 2D-GISAXS pattern. The low ordered morphologies observed at 14 h annealing time (Figure 4a,d) as compared to Janus-01 is probably due to higher content of oligosaccharide in the sample, which offer stronger hydrogen bonding, resulting in

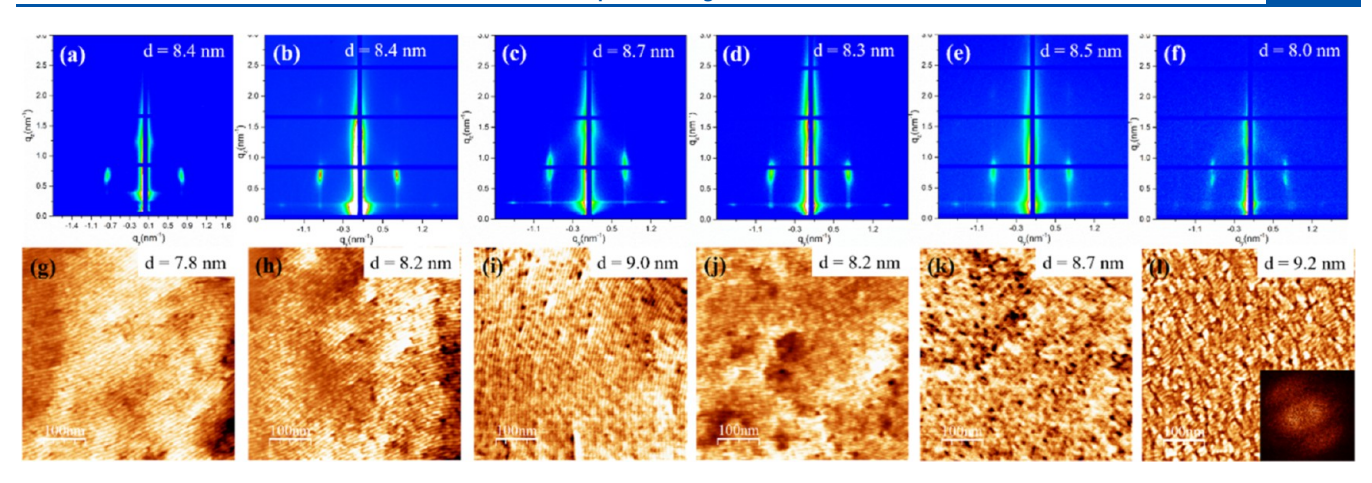


Figure 6. 2D-GISAXS of the PPSNb-BuMT-04 (Janus-04, Table 1) thin films annealed in different solvent vapor compositions and times: (a) THF/H₂O, 1:1, 14 h, (b) THF/H₂O, 1:1, 24 h, (c) THF/H₂O, 1:1, 60 h, (d) THF/H₂O, 3:1, 14 h, (e) THF/H₂O, 3:1, 24 h, and (f) THF/H₂O, 3:1, 60 h. (g-l) Their corresponding AFM images.

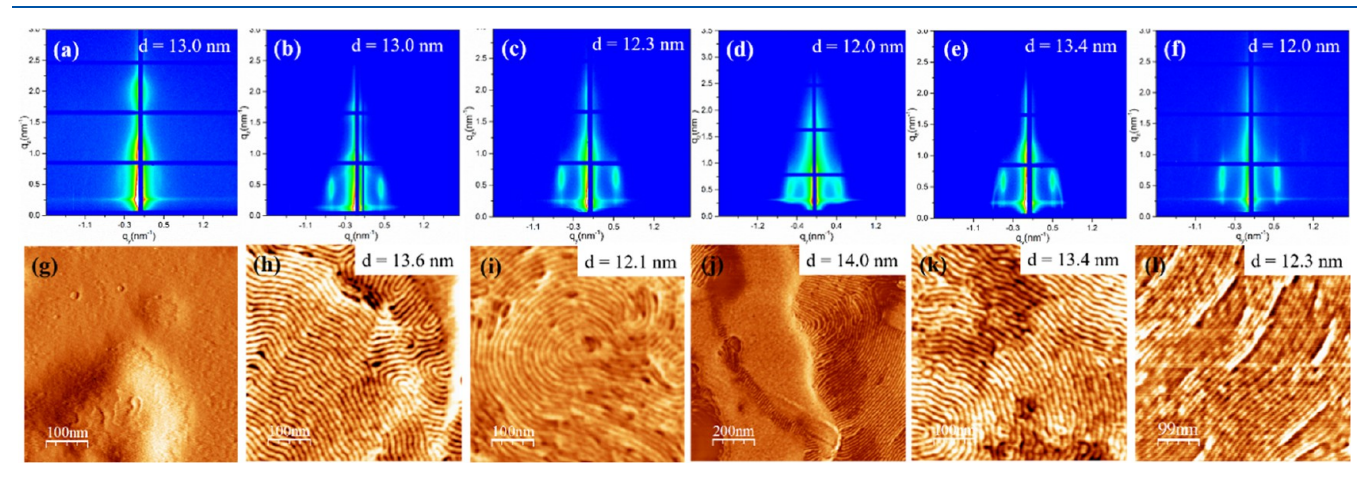


Figure 7. 2D-GISAXS of the PPSNb-BuMH-10 (Janus-10, Table 1) thin films annealed in different solvent vapor compositions and times: (a) THF/H₂O, 1:1, 14 h, (b) THF/H₂O, 1:1, 24 h, (c) THF/H₂O, 1:1, 60 h, (d) THF/H₂O, 3:1, 14 h, (e) THF/H₂O, 3:1, 24 h, and (f) THF/H₂O, 3:1, 60 h. (g-l) Their corresponding AFM images.

the less chain mobility. The higher order observed in the BBCP sample (Figure 4b) annealed for 24 h in 1:1 (wt/wt) THF/ H_2O mixture environment as compared to sample (Figure 4e) annealed for the same period in a 3:1 (wt/wt) THF/ H_2O mixture could also be explained by the presence of higher MH content, which like the H_2O richer environment results in improved BBCP chain mobility.

In order to further elaborate the effect of PS molecular weight on morphological behavior, thin films of the Janus BBCP (Janus-03, Table 1) having a PS branch with 5.5 kDa molecular weight (highest in this study) were prepared and treated in a similar fashion as mentioned above. The 2D-GISAXS patterns and corresponding AFM images (Figure 5) of these samples disclosed the existence of well-defined perpendicularly oriented cylinders except in one particular case where phase transition is observed (Figure 5f,l) at 60 h annealing. This is supported by the GISAXS intensity profile along q_v integrated around the Yoneda band, which exhibits a 1: $\sqrt{3}$ relative peak position ratio from the primary scattering peak q_{ν}^* , is consistent with an out-of-plane cylindrical structure. As it is clear from 2D-GISAXS patterns (Figure 5a-c) and corresponding AFM images (Figure 5g-i), the longer-range order of the HEX cylinders improves with the increasing annealing time in the 1:1 THF/H₂O solvent system,

which is also evident from enhancement in the sharpness of the scattering peaks at 60 h annealing time (Figure 50) and the corresponding two-dimensional Fast Fourier Transform (2D-FFT) profile. However, inverse effect was observed in 3:1 THF/H₂O SVA system, i.e., the longer-range order obtained at low annealing time (Figure 5d,j,p) due to higher chain mobility in PS rich sample and this longer range order decrease with inceasing annealing time until a start of phase transition process from HEX cylinders to cubic array take place after 60 h (Figure 5f,1). The PS swelled more in this THF-rich environment as compared oligosaccharide because of the increase in its volume fraction, which led to this phase transition. Nevertheless, the GISAXS intensity profile for this sample along q_y integrated around the Yoneda band still displays a 1: $\sqrt{3}$ relative peak position ratio from the primary scattering peak q_y^* , which indicates the presence of the HEX cylindrical structure, and the system seems to be in the process of the phase transition intermediate stage, which is also evident from the corresponding 2D-FFT profile (Figure 5r). A similar phase transition from HEX to cubic morphology was observed by Paik et al. during their study of the in situ swelling of poly(α -methylstyrene-block-4-hydroxystyrene) (P α MS-b-PHOST) thin films in acetone vapor, using a GISAXS instrument.33

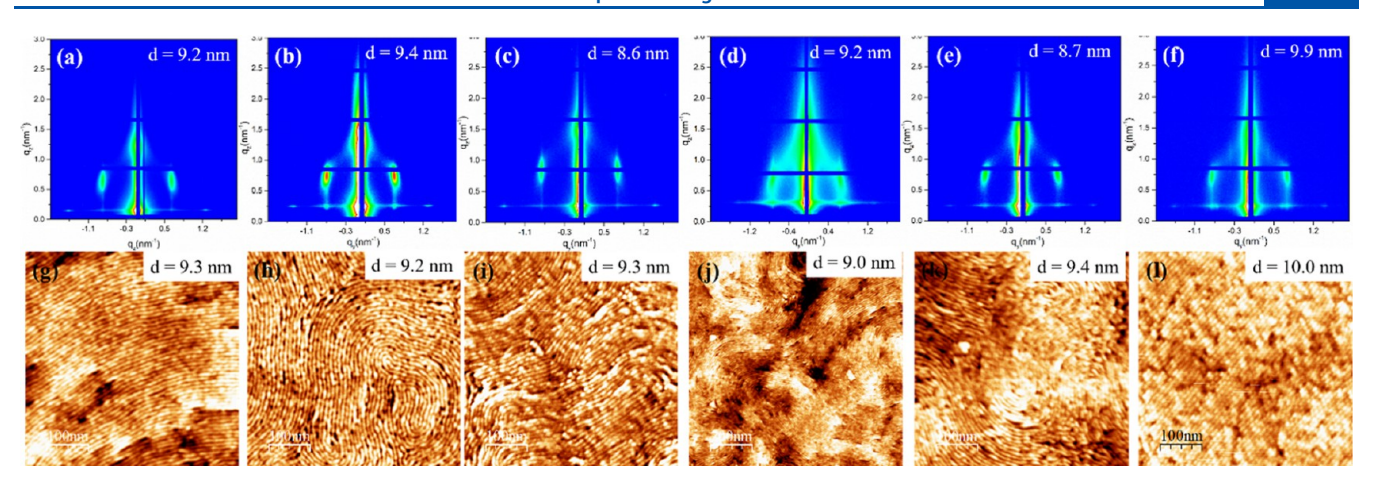


Figure 8. 2D-GISAXS of the PPSNb-BuMT-11 (Janus-11, Table 1) thin films annealed in different solvent vapor compositions and times: (a) THF/H₂O, 1:1, 14 h, (b) THF/H₂O, 1:1, 24 h, (c) THF/H₂O, 1:1, 60 h, (d) THF/H₂O, 3:1, 14 h, (e) THF/H₂O, 3:1, 24 h, and (f) THF/H₂O, 3:1, 60 h. (g-l) Their corresponding AFM images.

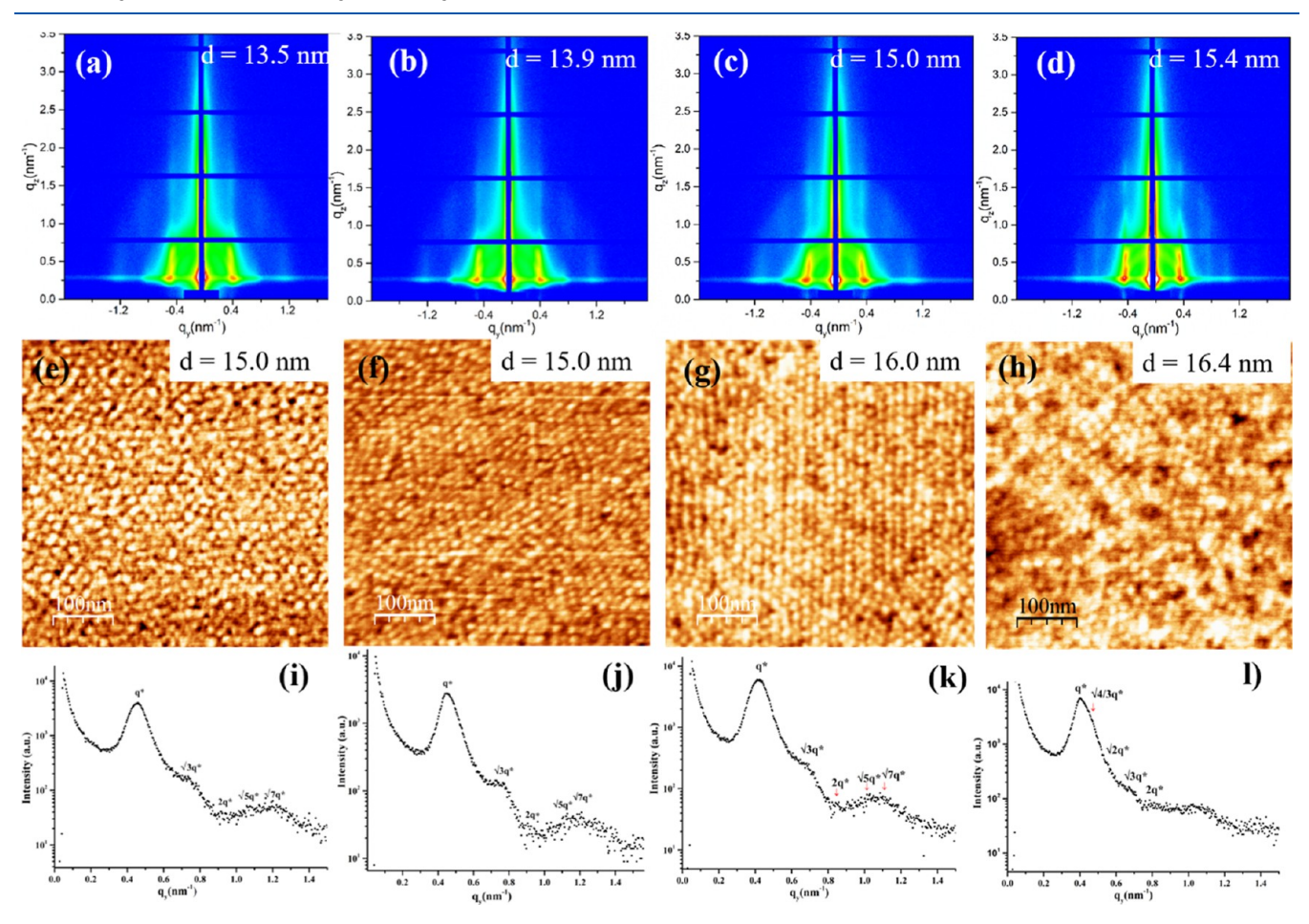


Figure 9. 2D-GISAXS of the PPSNb-BuMH-12 (Janus-12, Table 1) thin films annealed in different solvent vapor compositions and times: (a) THF/H₂O, 1:1, 14 h, (b) THF/H₂O, 1:1, 24 h, (c) THF/H₂O, 1:1, 48 h, and (d) THF/H₂O, 1:1 60 h. (e-h) Their corresponding AFM images and (i-l) their respective GISAXS intensity cuts along the horizontal q_{ν} direction taken around the Yoneda band.

When MH was replaced with MT containing only three glucose units and branching with smaller PS $(1.6~\mathrm{kDa})$ in Janus BBCP backbone, well-defined longer range ordered in-plane HEX cylindrical morphologies were obtained, as shown in the AFM images and 2D-GISAXS profiles (Figure 6). Similar to this, the organization of the cylindrical morphologies improves with annealing time in a $1:1~\mathrm{THF/H_2O}$ solvent vapor environment, which is evident from the appearance and

intensity of the second order scattering peak in its 2D-GISAXS profiles (Figure 6a–c). On the other hand, better organization was obtained at lower annealing time (Figure 6d) and a phase transition took place at 60 h (Figure 6f,l), probably due to the same reason as described above. The domain size as calculated from the primary peak of the corresponding GISAXS profiles is around 8 nm (4 nm half-pitch) and is consistent with their respective AFM values.

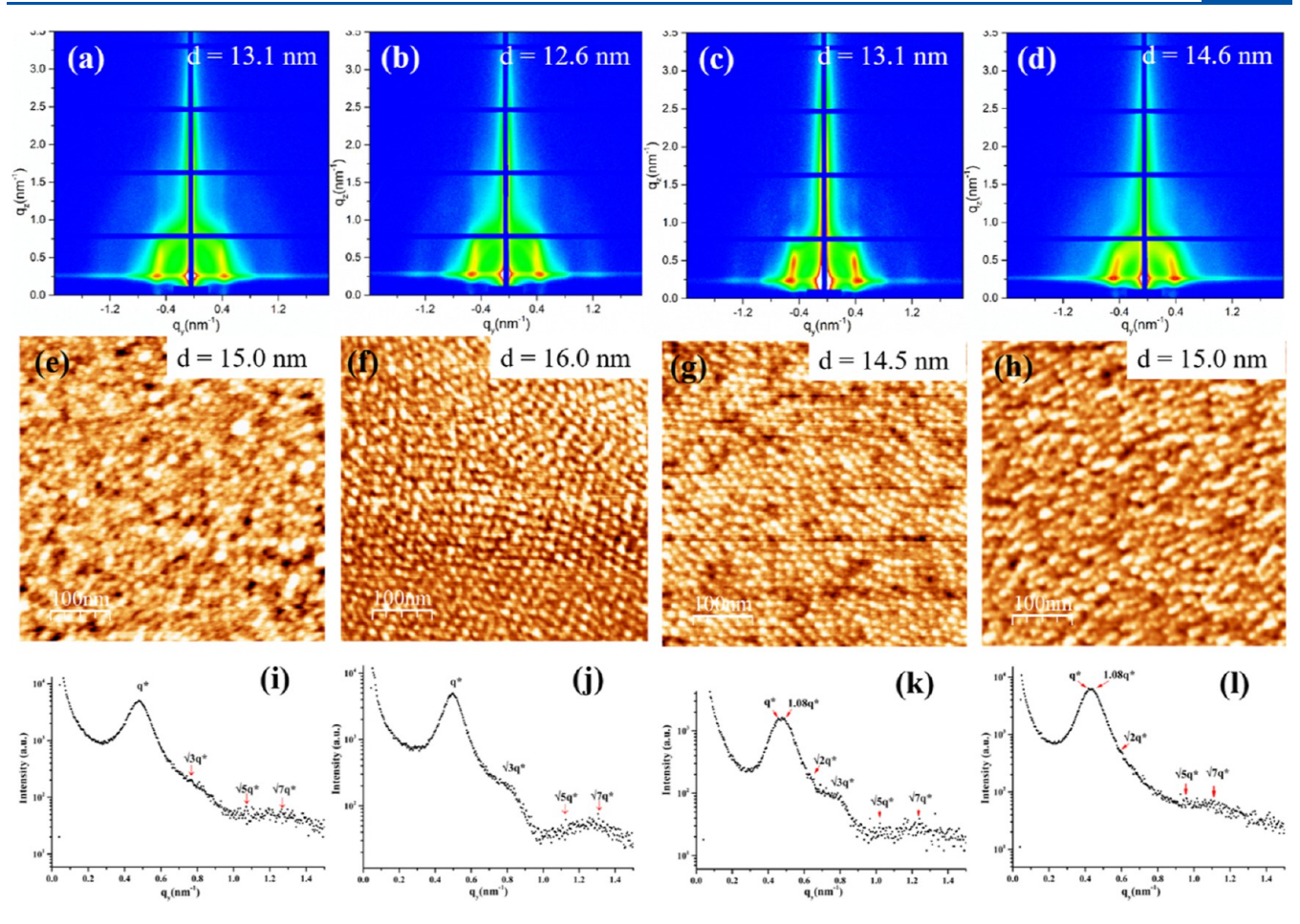


Figure 10. 2D-GISAXS of the PPSNb-BuMH-12 (Janus-12, Table 1) thin films annealed in different solvent vapor compositions and times: (a) THF/H₂O, 3:1, 14 h, (b) THF/H₂O, 3:1, 24 h, (c) THF/H₂O, 3:1, 48 h, and (d) THF/H₂O, 3:1 60 h. (e-h) Their corresponding AFM images and (i-l) their respective GISAXS intensity cuts along the horizontal q_{γ} direction taken around the Yoneda band.

The Janus BBCP samples described above with different PS and oligosaccharide branches have an overall DP of 25. In order to investigate the effect of a longer backbone on the self-assembly behavior, two additional Janus BBCP samples with the same PS branch ($M_n^{PS} = 1.6 \text{ kDa}$) but different oligosaccharides (MH or MT) (Janus-10 & 11, Table 1) and their thin films were annealed in similar conditions as mentioned above. The results of the self-segregation of these samples in their thin films, prepared in an identical environment as described above, are shown in Figures 7 and 8.

It is apparent from their 2D-GISAXS scattering profiles and AFM images that nearly identical results were obtained as for their shorter homologues (Janus-02 and 04). As is clear from Figure 7, lower morphological organization order was observed with the system having an MH branch (Janus-10) as compared to its smaller backbone counterpart (Janus-02, Figure 4), probably due to low mobility of BBCP with a longer backbone due to entanglement and stronger hydrogen bonding offered by MH. Conversely, nicely ordered in-plane HEX cylinders were obtained when MH was replaced by MT in Janus BBCP (Janus 11, Table 1), similar to its lower DP analogue (Janus 04, Figure 6), probably due to less resistance to mobility and hydrogen bonding offered by smaller MT. Additionally, an identical trend in morphological organization in different THF/H₂O solvent was observed. The clear splitting of the primary scattering peak in the 2D-GISAXS pattern and the appearance of dots in the AFM image of the sample exposed to

the 3:1 THF/ H_2O solvent environment for 60 h indicate the order-order phase transition, similar to the low DP counterpart.

Finally, the self-assemblies of the Janus BBCPs with intermediate molecular weight of PS branch (Janus 12, Table 1, $M_n^{PS} = 3$ kDa) were also investigated with an additional annealing time at 48 h, keeping all the conditions identical as described above. The 2D-GISAXS patterns and corresponding AFM phase images for the samples annealed in a 1:1 THF/ H₂O environment for 14-60 h are shown in Figure 9. The analysis of 2D-GISAXS patterns and the appearance of Bragg rods at the 1: $\sqrt{3}$:2: $\sqrt{5}$: $\sqrt{7}$ relative position with respect to primary scattering peaks along the Yoneda band elaborate the presence of hexagonally packed cylinders normal to the surface for the samples exposed to a 1:1 THF/H2O solvent vapor environment for 14-48 h (Figure 9a-c,i-k). As previously observed, the periodic organization improves with annealing time, which is also corroborated by the corresponding AFM images (Figure 9e-g). The nature and trend toward a higher degree of ordering, however, changes when extending the annealing time to 60 h. The decrease in the scattering intensity of higher order peaks corresponding to HEX morphologies and the appearance of a new pattern at the $1:\sqrt{4/3}:\sqrt{2}:\sqrt{3}:2$ relative position with respect to primary scattering peaks along the Yoneda band suggest the formation of the BCC morphology. This order-order phase transition was also confirmed by the presence of peaks at the $1:\sqrt{2}:\sqrt{5}$ relative

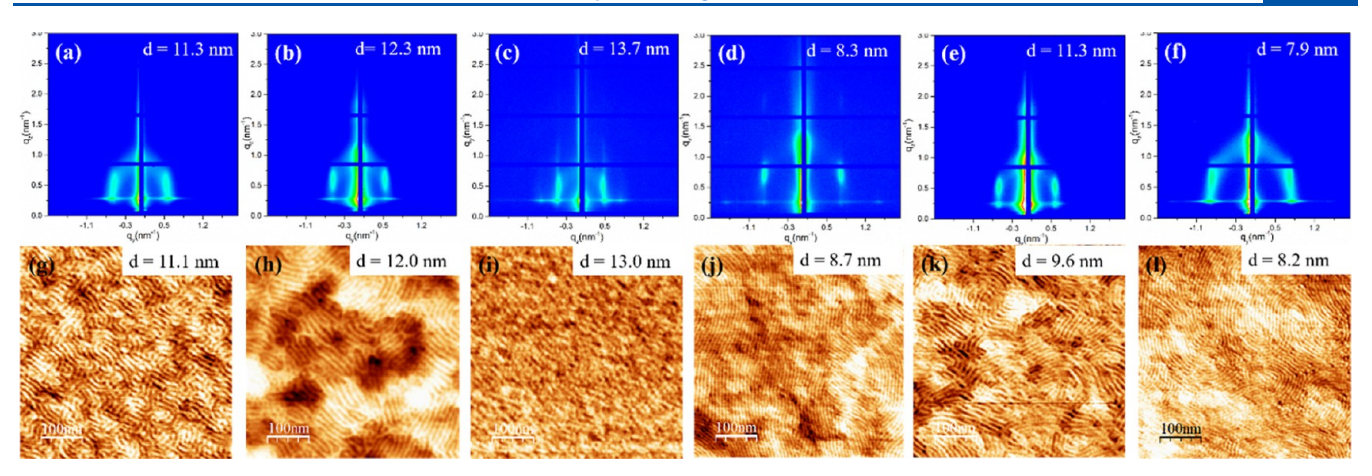


Figure 11. 2D-GISAXS profiles of Janus BBCP thin films annealed using HTSVA at 160 °C for 1 min in a 1:1 (wt/wt) THF/H₂O mixture solvent atmosphere. (a) Janus-01, Table 1, (b) Janus-02, Table 1, (c) Janus-03, Table 1, (d) Janus-04, Table 1, (e) Janus-10, Table 1, (f) Janus-11, Table 1, and (g-l) their AFM images.

position in the GISAXS intensity cut along the q_z direction extracted at q_y *(Figure S12). Additionally, the domain size of the nanofeatures increases from 14 to 15.4 nm (1.1x HEX)³⁴ by increasing the annealing time from 48 to 60 h, which also supports HEX—BCC phase transition.

When Janus-12 BBCP thin films were annealed in a 3:1 THF/H₂O solvent mixture atmosphere, perpendicularly oriented cylinders were observed at 14-24 h annealing time, as revealed by 2D-GISAXS patterns and intensity cuts profile along the Yoneda band in the q_v direction (Figure 10a,b,i,j). The orientation order improves with annealing time, as also indicated by their corresponding AFM images (Figure 10e,f). The splitting of primary scattering into two at the 1:1.08 relative peak in the 2D-GISAXS patterns of the thin films annealed for 48 h is typical of FCC morphology, which indicates the intermediate stage of transition from HEX-FCC, as scattering peaks dedicated to HEX morphology are still present. This early start in transition as compared to the 1:1 THF/H₂O solvent mixture is due to rapid swelling of PS in the THF-dominant environment. The dramatic decrease in scattering intensity of higher order peaks and appearance of Debye-Scherrer rings in the 2D-GISAXS profile (Figure 10d,l) for the sample annealed at 60 h indicate the random orientation or start of disordering in periodic structures, which is also corroborated by the presence of disarray features in the AFM image (Figure 10h).

Although the conventional solvent annealing process as described above is easy to perform, does not need any sophisticated instrumentation, and could be started in a beaker, it is time-consuming and probably not good for large-scale industrial application. In order to accelerate the annealing process, our group reported a fast-ordering method, termed HTSVA, and showed that the HTSVA provided an ideal binary solvent vapor environment at a high temperature using microwave energy that achieved the self-assembly of linear MH-*b*-PS in 1 s. The HTSVA when applied on Janus BBCPs in identical solvent mixtures as described, well-defined, periodic nanofeatures were obtained in only 1 min (Figures 11 and S13, 14).

As is clear from 2D-GISAXS patterns and their corresponding AFM images, identical self-assemblies were obtained in 1 min using HTSVA at 160 °C using μ -wave energy, which were otherwise achieved in 14–60 h using the conventional solvent annealing approach. The periodic organization could be further

improved by playing with the annealing time and $\mathrm{THF}/\mathrm{H}_2\mathrm{O}$ solvent environment.

From the above results, it is clear that in-plane morphologies are achieved with a low molecular weight PS block (1.5–2 kDa) due to preferential wetting of the hydrophilic substrate with carbohydrate segments of BBCPs, which is a common phenomenon where the incompatibility between two components of the block copolymers is high (high χ block copolymers). As the molecular weight of the PS increases (3–5.5 kDa in this case), the carbohydrate segments become increasingly confined, preventing their preferential wetting of the hydrophilic substrate and leading to an out-of-plane structure.

CONCLUSIONS

In summary, we successfully synthesized high χ PS-branch-Oligosaccharides Janus-type bottle brush copolymers with varying compositions and degrees of polymerization with narrow dispersities using an original, simple, and scalable approach. These Janus-type BBCPs self-segregate to give longer range order, ultrasmall periodic nanodomains down to sub-5 nm, under SVA. The orientations of nanofeatures depend upon the molecular weight of PS side chain for a given oligosaccharide branch. The out of plane cylindrical morphologies are obtained for 3 and 5.5 kDa and horizontally oriented cylinders were observed for lower molecular weight (1.5–2 kDa) PS side chains while using MH as another branch in Janus BBCPs. A very fast ordering (in 1 min) was obtained under HTSVA using microwave energy as compared to conventional solvent annealing at room temperature (14-60 h). The transition from HEX to cubic morphologies took place, when thin films were exposed to a 3:1(wt/wt) THF/ H₂O SVA system for 48-60 h due to preferential swelling of PS by THF-rich solvent vapors, which result in the change of volume fraction of the copolymers, which should be responsible for this order to order transition. Here, we have focused our effort on carbohydrate materials, using at least one moiety as a side chain; otherwise, our versatile approach could be easily used to prepare Janus BBCPs in only two steps, which make it the simplest way to produce Janus BBCPs ever reported.

Additionally, this strategy could be applied to diverse polymer systems. Finally, the domain size in our original Janus-

type BBCPs system could be further reduced by further decreasing the PS molecular weight and replacing MH and MT with lower molecular weight carbohydrate such as maltose and glucose.

ASSOCIATED CONTENT

5 Supporting Information

The Supporting Information is available free of charge at https://pubs.acs.org/doi/10.1021/acs.macromol.4c00390.

Experimental procedures, materials, ¹H NMR spectra for all compounds, FTIR spectra, tables of results, 2D-GISAXS images, AFM images, and SEC traces (PDF)

AUTHOR INFORMATION

Corresponding Authors

Muhammad Mumtaz — University of Grenoble Alpes, CNRS, CERMAV, Grenoble 38000, France; orcid.org/0009-0008-2810-3067; Email: cmmumtaz@gmail.com

Redouane Borsali — University of Grenoble Alpes, CNRS, CERMAV, Grenoble 38000, France; orcid.org/0000-0002-7245-586X; Email: redouane.borsali@cermav.cnrs.fr

Authors

Daniel Hermida Merino — Dutch-Belgian Beamline, Netherlands Organization for Scientific Research, European Synchrotron Radiation Facility, Grenoble F-38000, France; Departamento de Física Aplicada, Universidade de Vigo, Campus Lagoas-Marcosende, Vigo E-36310 Galicia, Spain

Eduardo Solano — NCD-SWEET Beamline, ALBA Synchrotron Light Source, Cerdanyola del Valles 08290, Spain; orcid.org/0000-0002-2348-2271

Wen-Chang Chen – Department of Chemical Engineering, National Taiwan University, Taipei 10617, Taiwan; Advanced Research Center for Green Materials Science and Technology, National Taiwan University, Taipei 10617, Taiwan; orcid.org/0000-0003-3170-7220

Complete contact information is available at: https://pubs.acs.org/10.1021/acs.macromol.4c00390

Author Contributions

M.M. conceived, designed, and performed the experiments and wrote the original draft. D.-H.M. and E.S. performed 2D-GISAXS analysis. W.-C.C. contributed to the discussions of the results and R.B. conceptualized the study, contributed to the discussions of the results, managed the project, and acquired funding. All authors have given approval to the final version of the manuscript.

Notes

The authors declare no competing financial interest.

ACKNOWLEDGMENTS

The authors are grateful to CNRS, Univ. Grenoble Alpes, and NTU for their financial support of the IRP (International Research Project Green Material Institute- France-Taiwan) and PolyNat Carnot Institut, Grenoble, France. GISAXS measurements were performed at: NCD-SWEET beamline at ALBA synchrotron with the collaboration with ALBA staff." D.H.-M. acknowledges the "María Zambrano" contract of the University of Vigo, financed by the Spanish Ministerio de Universidades/33.50.460A.752 and by "European Union NextGenerationEU/PRTR."

REFERENCES

- (1) Albert, J. N. L.; Epps, T. H. Self-assembly of block copolymer thin films. *Mater. Today* **2010**, *13* (6), 24–33.
- (2) Matsen, M. W. Effect of Architecture on the Phase Behavior of AB-Type Block Copolymer Melts. *Macromolecules* **2012**, *45* (4), 2161–2165.
- (3) Mansky, P.; haikin, P.; Thomas, E. L. Monolayer films of diblock copolymer microdomains for nanolithographic applications. *J. Mater. Sci.* 1995, 30 (8), 1987–1992.
- (4) Cushen, J. D.; Otsuka, I.; Bates, C. M.; Halila, S.; Fort, S.; Rochas, C.; Easley, J. A.; Rausch, E. L.; Thio, A.; Borsali, R.; Willson, C. G.; Ellison, C. J. Oligosaccharide/Silicon-Containing Block Copolymers with 5 nm Features for Lithographic Applications. *ACS Nano* 2012, 6 (4), 3424–3433.
- (5) Hung, C.-C.; Chiu, Y.-C.; Wu, H.-C.; Lu, C.; Bouilhac, C.; Otsuka, I.; Halila, S.; Borsali, R.; Tung, S.-H.; Chen, W.-C. Conception of stretchable resistive memory devices based on nanostructure-controlled carbohydrate-block-polyisoprene block copolymers. *Adv. Funct. Mater.* **2017**, *27* (13), 1606161.
- (6) Yoo, H. G.; Byun, M.; Jeong, C. K.; Lee, K. J. Performance enhancement of electronic and energy devices via block copolymer self-assembly. *Adv. Mater.* **2015**, *27* (27), 3982–3998.
- (7) Chiu, Y.-C.; Otsuka, I.; Halila, S.; Borsali, R.; Chen, W.-C. High performance nonvolatile transistor memories of pentacence using the green electrets of sugar-based block copolymers and their supramolecules. *Adv. Funct. Mater.* **2014**, 24 (27), 4240–4249.
- (8) Darling, S. B. Block copolymers for photovoltaics. *Energy Environ. Sci.* **2009**, 2 (12), 1266–1273.
- (9) Wang, M.; Wudl, F. Top-down meets bottom-up: organized donor-acceptor heterojunctions for organic solar cells. *J. Mater. Chem.* **2012**, 22 (46), 24297–24314.
- (10) Fasolka, M. J.; Mayes, A. M. Block copolymer thin films: Physics and applications. *Annu. Rev. Mater. Res.* **2001**, *31*, 323–355.
- (11) Aissou, K.; Halila, S.; Fort, S.; Borsali, R.; Baron, T. Thin Films Organized in Nanodomains on the Basis of Copolymers Having Polysaccharide Blocks for Applications in Nanotechnology. U.S. Patent 20,130,189,609 B2, 2013.
- (12) Sheiko, S. S.; Sumerlin, B. S.; Matyjaszewski, K. Cylindrical molecular brushes: Synthesis, characterization, and properties. *Prog. Polym. Sci.* **2008**, 33 (7), 759–785.
- (13) Xia, Y.; Olsen, B. D.; Kornfield, J. A.; Grubbs, R. H. Efficient Synthesis of Narrowly Dispersed Brush Copolymers and Study of Their Assemblies: The Importance of Side Chain Arrangement. *J. Am. Chem. Soc.* **2009**, *131* (51), 18525–18532.
- (14) Gu, W.; Huh, J.; Hong, S. W.; Sveinbjornsson, B. R.; Park, C.; Grubbs, R. H.; Russell, T. P. Self-Assembly of Symmetric Brush Diblock Copolymers. *ACS Nano* **2013**, *7* (3), 2551–2558.
- (15) Rzayev, J. Synthesis of Polystyrene-Polylactide Bottlebrush Block Copolymers and Their Melt Self-Assembly into Large Domain Nanostructures. *Macromolecules* **2009**, *42* (6), 2135–2141.
- (16) Dalsin, S. J.; Rions-Maehren, T. G.; Beam, M. D.; Bates, F. S.; Hillmyer, M. A.; Matsen, M. W. Bottlebrush Block Polymers: Quantitative Theory and Experiments. *ACS Nano* **2015**, *9* (12), 12233–12245.
- (17) Sveinbjornsson, B. R.; Weitekamp, R. A.; Miyake, G. M.; Xia, Y.; Atwater, H. A.; Grubbs, R. H. Rapid self-assembly of brush block copolymers to photonic crystals. *Proc. Natl. Acad. Sci. U.S.A.* **2012**, 109 (36), 14332–14336.
- (18) Miyake, G. M.; Piunova, V. A.; Weitekamp, R. A.; Grubbs, R. H. Precisely tunable photonic crystals from rapidly self-assembling brush block copolymer blends. *Angew. Chem., Int. Ed.* **2012**, *51* (45), 11246–11248.
- (19) Mumtaz, M.; Takagi, Y.; Mamiya, H.; Tajima, K.; Bouilhac, C.; Isono, T.; Satoh, T.; Borsali, R. Sweet Pluronic poly (propylene oxide)-b-oligosaccharide block copolymer systems: Toward sub-4 nm thin-film nanopattern resolution. *Eur. Polym. J.* **2020**, *134*, 109831.
- (20) Aissou, K.; Mumtaz, M.; Fleury, G.; Portale, G.; Navarro, C.; Cloutet, E.; Brochon, C.; Ross, C. A.; Hadziioannou, G. Sub-10 nm Features Obtained from Directed Self-Assembly of Semicrystalline

- Polycarbosilane-Based Block Copolymer Thin Films. *Adv. Mater.* **2015**, *27* (2), 261–265.
- (21) Cushen, J. D.; Bates, C. M.; Rausch, E. L.; Dean, L. M.; Zhou, S. X.; Willson, C. G.; Ellison, C. J. Thin Film Self-Assembly of Poly(trimethylsilylstyrene-b-d,l-lactide) with Sub-10 nm Domains. *Macromolecules* **2012**, 45 (21), 8722–8728.
- (22) Rodwogin, M. D.; Spanjers, C. S.; Leighton, C.; Hillmyer, M. A. Polylactide—Poly(dimethylsiloxane)—Polylactide Triblock Copolymers as Multifunctional Materials for Nanolithographic Applications. *ACS Nano* **2010**, *4* (2), 725–732.
- (23) Kennemur, J. G.; Yao, L.; Bates, F. S.; Hillmyer, M. A. Sub-5 nm Domains in Ordered Poly(cyclohexylethylene)-block-poly (methyl methacrylate) Block Polymers for Lithography. *Macromolecules* **2014**, *47* (4), 1411–1418.
- (24) Sweat, D. P.; Kim, M.; Larson, S. R.; Choi, J. W.; Choo, Y.; Osuji, C. O.; Gopalan, P. Rational Design of a Block Copolymer with a High Interaction Parameter. *Macromolecules* **2014**, *47* (19), 6687–6696.
- (25) Ding, S.-P.; Zhang, Z.-K.; Ye, Z.; Du, B.-Y.; Xu, J.-T. Fabrication of High χ -Low N Block Copolymers with Thermally Stable Sub-5 nm Microdomains Using Polyzwitterion as a Constituent Block. ACS Macro Lett. **2021**, 10 (10), 1321–1325.
- (26) Lane, A. P.; Yang, X.; Maher, M. J.; Blachut, G.; Asano, Y.; Someya, Y.; Mallavarapu, A.; Sirard, S. M.; Ellison, C. J.; Willson, C. G. Directed Self-Assembly and Pattern Transfer of Five Nanometer Block Copolymer Lamellae. *ACS Nano* **2017**, *11* (8), 7656–7665.
- (27) Guo, Z.; Le, A. N.; Feng, X.; Choo, Y.; Liu, B.; Wang, D.; Wan, Z.; Gu, Y.; Zhao, J.; Li, V.; Osuji, C. O.; Johnson, J. A.; Zhong, M. Janus Graft Block Copolymers: Design of a Polymer Architecture for Independently Tuned Nanostructures and Polymer Properties. *Angew. Chem., Int. Ed.* **2018**, 57 (28), 8493–8497.
- (28) Nguyen, H. V.-T.; Gallagher, N. M.; Vohidov, F.; Jiang, Y.; Kawamoto, K.; Zhang, H.; Park, J. V.; Huang, Z.; Ottaviani, M. F.; Rajca, A.; Johnson, J. A. Scalable Synthesis of Multivalent Macromonomers for ROMP. *ACS Macro Lett.* **2018**, 7 (4), 472–476.
- (29) Kawamoto, K.; Zhong, M.; Gadelrab, K. R.; Cheng, L. C.; Ross, C. A.; Alexander-Katz, A.; Johnson, J. A. Graft-through synthesis and assembly of Janus bottlebrush polymers from A-Branch-B diblock macromonomers. *J. Am. Chem. Soc.* **2016**, 138 (36), 11501–11504.
- (30) Xu, B.; Feng, C.; Huang, X. A versatile platform for precise synthesis of asymmetric molecular brush in one shot. *Nat. Commun.* **2017**, *8*, 333.
- (31) Cheng, L.-C.; Gadelrab, K. R.; Kawamoto, K.; Yager, K. G.; Johnson, J. A.; Alexander-Katz, A.; Ross, C. A. Templated Self-Assembly of a PS-Branch-PDMS Bottlebrush Copolymer. *Nano Lett.* **2018**, *18* (7), 4360–4369.
- (32) Liao, Y.; Chen, W.-C.; Borsali, R. Carbohydrate-Based block copolymer thin films: ultrafast nano-organization with 7 nm resolution using microwave energy. *Adv. Mater.* **2017**, 29 (35), 1701645.
- (33) Paik, M. Y.; Bosworth, J. K.; Smilges, D.-M.; Schwartz, E. L.; Andre, X.; Ober, C. K. Reversible Morphology Control in Block Copolymer Films via Solvent Vapor Processing: An in Situ GISAXS Study. *Macromolecules* **2010**, 43 (9), 4253–4260.
- (34) Matsen, M. W. Cylinder ↔ Sphere Epitaxial Transitions in Block Copolymer Melts. J. Chem. Phys. 2001, 114 (18), 8165–8173.